2022

The Effect of Corrosion Protection Methods on The Thermal-Hydraulic Performance of Aluminum Microchannel Heat Exchangers

Yupeng Wang

Hui Zhao

Pega Hrnjak

The Effects of External Corrosion Protection Methods on the Thermal-Hydraulic Performance of Aluminum Microchannel Heat Exchangers

Yupeng WANG[(1)], Hui ZHAO[(1,2)], Pega HRNJAK[(1,2,*)]

[1]University of Illinois at Urbana-Champaign
Department of Mechanical Science and Engineering
1206 West Green Street, Urbana, IL 61801, USA

[2]Creative Thermal Solutions, Inc.
2209 North Willow Road, Urbana, IL 61802, USA

* Corresponding author: pega@illinois.edu

ABSTRACT

Aluminum microchannel heat exchangers are widely used in heating and cooling applications owing to their superior thermal performance and lightweight structure. The various working environments impose challenges on the corrosion resistance of the heat exchangers. Applying coating on the external surface of the heat exchangers has been one of the common methods to enhance their resistance to external corrosion. This paper presents the effects of corrosion simulated by an accelerated corrosion test on the thermal-hydraulic performance of three otherwise identical brazed aluminum heat exchangers with different surface treatments: the first heat exchanger with no treatment; the second with an organic electrophoretic coating (E-coating); and the third with conversion coating by a trivalent chromium process (TCP). The mass and thermal-hydraulic performance of the heat exchangers are evaluated before and after the exposure to a ten-day laboratory cyclic salt fog corrosion test. The result shows that due to the relatively thicker E-coating film, the initial performance of the E-coated heat exchanger is inferior to both the uncoated and TCP-coated heat exchangers. After the ten-day corrosion test, it is visually observed that the E-coating provides better protection to the heat exchanger than the TCP coating in the salt fog environment. No visible geometric deformation and fin-tube debonding are observed on the E-coated heat exchanger, while the uncoated and the TCP-coated heat exchangers show a certain level of deformation and fin-tube debonding. After the corrosion test, the uncoated heat exchanger shows a large performance degradation: the airside pressure drop increases by up to 13% and the UA decreases by up to 74% with the same frontal air velocity. The TCP-coated heat exchanger shows no significant change in airside pressure drop but an up to 61% decrease in UA. The E-coated heat exchanger shows very little change in performance after the current corrosion test.

1. INTRODUCTION

Brazed aluminum heat exchangers are subject to external corrosion when exposed to operating environments. A study on brazed aluminum automobile heat exchangers collected from field service shows various kinds of corrosion attacks on the fins, tubes, and braze joints of the heat exchangers (Melander & Woods, 2010). Accelerated laboratory corrosion test ASTM G85:A3, also called SWAAT, is commonly used in the automotive industry to evaluate the corrosion resistance of the brazed aluminum heat exchangers. Scott *et al.* (1997) compared several accelerated corrosion tests and showed that the SWAAT test can reasonably replicate the corrosion behaviors of brazed aluminum heat exchangers from field service in some geographic locations.

To protect the aluminum MCHEs from external corrosion, various coatings have been applied on the external surface of heat exchangers. Organic electrocoating (e-coating) is one of the commonly used anti-corrosion coatings. The coating is applied by an electrophoretic dipping process and works as a barrier on the metal substrate against the external environments. The effectiveness of e-coating under various laboratory test conditions has been demonstrated

in existing studies (Ainali *et al*., 1993; Fedrizzi *et al*., 2008). The trivalent chromium process (TCP) is another coating technology that has been applied on aluminum substrates to enhance corrosion resistance. During the process, a double-layer coating structure consisting of the oxide compound of aluminum, chromium, and zirconium is formed on the surface of the aluminum (Qi *et al*., 2015; Munson & Swain, 2017). The TCP coating has shown good corrosion protection ability on aluminum alloys in some laboratory corrosion tests (Munson *et al*., 2018; Walton *et al*., 2019).

External corrosion of heat exchangers not only reduces the mechanical integrity (e.g., tube pitting, loss of fin materials) but also causes degradation of the thermal-hydraulic performance (Wang *et al*., 2021). This paper presents the effects of corrosion generated by an accelerated corrosion test on the thermal-hydraulic performance of brazed aluminum microchannel heat exchangers (MCHEs). In the experiment, three aluminum MCHEs with identical heat exchanger cores but different surface treatments, one uncoated, one with TCP coating, and one with e-coating, are evaluated before and after the exposure to ten days of SWAAT following the procedure of Wang *et al*. (2021). The impact of coatings on the heat exchanger performance before and after corrosion tests are evaluated and compared with the heat exchanger without coating.

2. EXPERIMENTAL METHODS

2.1 Microchannel Heat Exchanger Samples

Three MCHEs with different protection methods are examined in this study, as illustrated in Figure 1. One heat exchanger does not have any coating applied, see Figure 1(a), it is called bare HX in this paper. The other two heat exchangers are applied with a TCP coating and an e-coating, respectively. The TCP-coated heat exchanger and the e-coated heat exchanger are illustrated in Figures 1(b) and 1(c), respectively. The three heat exchangers are otherwise identical except for the corrosion protection methods. Fin samples from each heat exchanger were carefully cut off and examined with an optical microscope. The measured thickness of the fin on the MCHEs is 0.08 mm. The thickness of chromium conversion coating on TCP-coated HX is too small to be measured from the current cross-section images. The measured thickness of the e-coating on the examined fin sample is up to 0.09 mm. Other key dimensions of the bare HX are listed in Table 1.

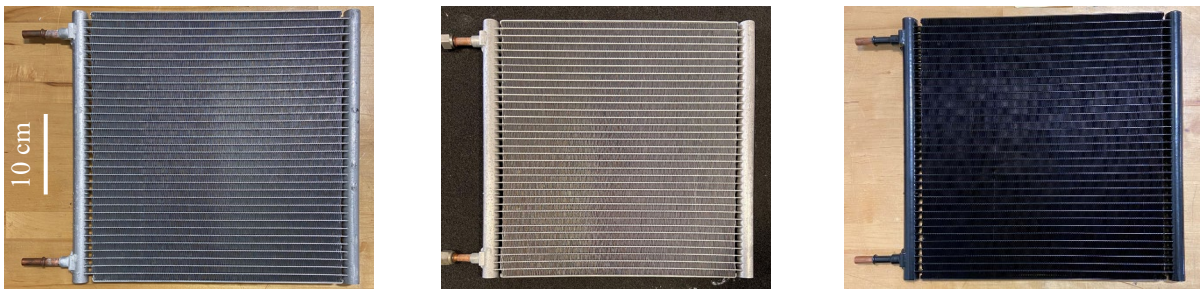

(a) (b) (c)

Figure 1: Photos of the MCHE samples: (a) bare HX; (b) TCP-coated HX (c) E-coated HX;

Table 1: Dimensions of the bare HX

Frontal face length	Frontal face height	Fin height	Fin pitch	Fin depth	Louver angle
[mm]	[mm]	[mm]	[mm]	[mm]	[degree]
304	330	8	1	16	26

2.2 Accelerated Corrosion Tests on Heat Exchangers

After the initial evaluation of the thermal performance of the as-received heat exchangers, ten-day continuous SWAAT (ASTM G85 Annex 3) tests are applied to all MCHE samples in a corrosion testing chamber. During the corrosion tests, the MCHE samples are pressurized with nitrogen and the pressure is monitored. There is no apparent pressure reduction observed throughout the test. It indicates no leak due to corrosion occurred during the ten-day corrosion test. The experimental setup is illustrated in Figure 2. After the corrosion tests, the MCHE samples are dried quiescently at room temperature. Then, they are cleaned by immersing in 5wt% nitric acid solution for up to 3 minutes to remove salt deposits and corrosion products. The purpose and effectiveness of the cleaning procedure have been discussed in a previous study (Wang *et al*., 2021).

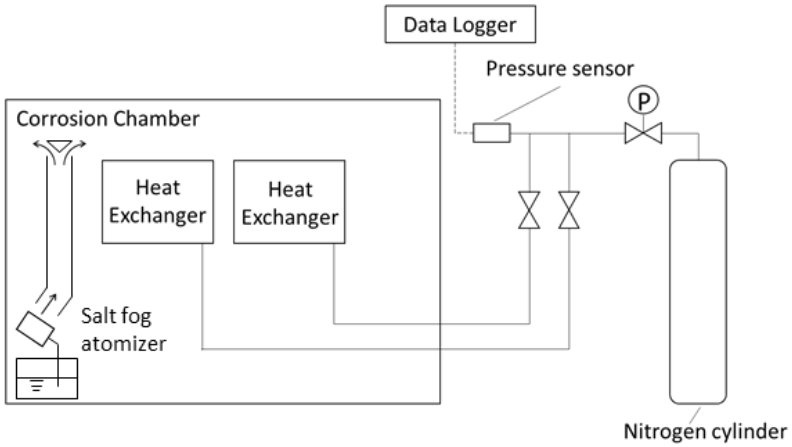

Figure 2: Schematic of the heat exchanger corrosion test setup

2.3 Evaluation of Heat Exchanger Thermal-hydraulic Performance

The thermal-hydraulic performance of the MCHE samples is evaluated in a wind tunnel before and after the corrosion tests. A schematic of the wind tunnel is shown in Figure 3. In the performance evaluation, air at room temperature is introduced into the wind tunnel by a centrifugal blower and heated by the MCHE sample. The hot water flows through the microchannel tube and is cooled by the external airflow. An immersion electric heater provided a constant heating capacity to the water flow. The airside pressure drop at the heat exchanger and the nozzle are measured by the differential pressure transducers. The air temperature is measured at the inlet and outlet of the heat exchanger, as well as at the outlet of the nozzle. The water temperature is measured at the inlet and outlet of the tube side of the heat exchanger. T-type thermocouples are used for all temperature measurements. The airflow rates are calculated based on the temperature and air pressure difference measurements at the nozzles (ASHRAE 41.2-18, 2018). The water mass flow rate is measured with a Coriolis meter. The uncertainty with the 95% confidence level of the measurements is listed in Table 2.

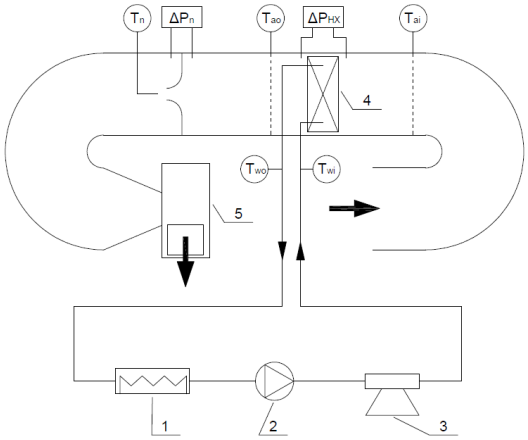

Figure 3: Schematic of the wind tunnel: 1 water heater; 2 water pump; 3 Coriolis meter; 4 heat exchanger sample; 5 air blower

Table 2: Uncertainty of measurements

Measured variables	Instruments	Uncertainty
T_a, T_w	T type thermocouple	± 0.1 ℃
$\dot{M}_w$	Coriolis flowmeter	$\pm 0.1\%$ of the measured value
ΔP_a	Pressure difference transmitter	$\pm 0.137\ Pa$ (±0.11% of full range)
ΔP_n	Pressure difference transmitter	$\pm 0.187\ Pa$ (±0.02% of full range)

The waterside heating capacity is kept at around $1000\ W$. Three nominal frontal air velocities are applied in the performance evaluation, which are 1.1, 1.4, and 1.8 m/s. The water mass flow is kept constant at 56 g/s. The airside capacity $\dot{Q}_a$ and the water-side capacity $\dot{Q}_w$ are calculated using Eq.(1) and Eq.(2), respectively.

$$\dot{Q}_a = \dot{M}_a(h_{ao} - h_{ai}) \tag{1}$$

$$\dot{Q}_w = \dot{M}_w(h_{wi} - h_{wo}) \tag{2}$$

The thermal balance, defined by Eq.(3) is within ±4%.

$$\Delta\dot{Q} = \frac{|\dot{Q}_a - \dot{Q}_w|}{\frac{1}{2}(\dot{Q}_a + \dot{Q}_w)} \times 100\% \tag{3}$$

The product of the overall heat transfer coefficient and heat transfer area UA is calculated using the $\varepsilon - NTU$ method for unmixed-unmixed cross-flow heat exchanger (Mills, 1999).

$$UA = NTU \cdot C_{min} \tag{4}$$

$$\varepsilon = \left\{ \frac{NTU^{0.22}}{C_{min}/C_{max}} \left[\exp\left(-\frac{C_{min}}{C_{max}} NTU^{0.78} \right) - 1 \right] \right\}^{-1} \tag{5}$$

The maximum and minimum flow-stream capacity rates, C_{min} and C_{max} are:

$$C_{max} = \dot{M}_w c_{p,w} \tag{6}$$

$$C_{min} = \dot{M}_a c_{p,a} \tag{7}$$

The measured and calculated uncertainty of airside pressure drop and UA of three MCHEs are listed in Table 3.

Table 3: Uncertainty of airside pressure drop and UA of three MCHEs

Time of evaluation	Frontal air velocity	Bare HX		TCP-coated HX		E-coated HX	
		Uncertainty of ΔP_a	Uncertainty of UA	Uncertainty of ΔP_a	Uncertainty of UA	Uncertainty of ΔP_a	Uncertainty of UA
	[m/s]	[%]	[%]	[%]	[%]	[%]	[%]
Before SWAAT	1.1	±0.9	±2.8	±0.9	±3.2	±0.8	±3.3
	1.4	±0.6	±3.0	±0.6	±3.0	±0.5	±3.1
	1.8	±0.5	±3.1	±0.5	±3.0	±0.4	±3.1
After SWAAT	1.1	±0.9	±2.1	±0.9	±2.1	±0.8	±3.4
	1.4	±0.5	±2.0	±0.6	±2.1	±0.5	±3.1
	1.8	±0.4	±2.0	±0.5	±2.1	±0.4	±3.1

3. RESULTS AND DISCUSSION

3.1 Visual Examination of MCHEs after Corrosion Tests

After the ten-day SWAAT test, significant deformation is observed on the bare and TCP-coated HXs. Figure 4 shows the three heat exchangers after the corrosion tests. It can be seen that the top and bottom rows of fins of the bare HX are completely detached from the HX core, see Figure 4(a). The height of the bare HX (excluding the two rows of fins that are detached from the core) increases from an initial 308 mm to 334 mm after the corrosion test. A close examination of the heat exchanger reveals that fin/tube debonding due to corrosion of brazed joints occurs at many locations on each row of fins on the bare HX. The lack of joints at these locations can be visually observed with the assistance of proper illumination from the backside of the heat exchanger. The schematic illustration of the visual inspection method is given in Figure 5. Similar to the bare HX, the TCP-coated HX also deforms but to a lesser extent, see Figure 4(b). The top and bottom rows of fins of the TCP-coated HX are also completely detached from the HX core. The height of the TCP-coated HX (excludes the two rows of detached fins) increases from 308 mm to 322 mm after the corrosion test. Fin/tube debonding is also observed at various locations. But the percentage of completely lost fin/tube braze joints on the TCP-coated HX (21%) is less than that on the bare HX (33%) based on an estimation from the careful visual inspection. For the E-coated HX, neither overall HX deformation nor fin/tube debonding has been identified after the corrosion test, see Figure 4(c).

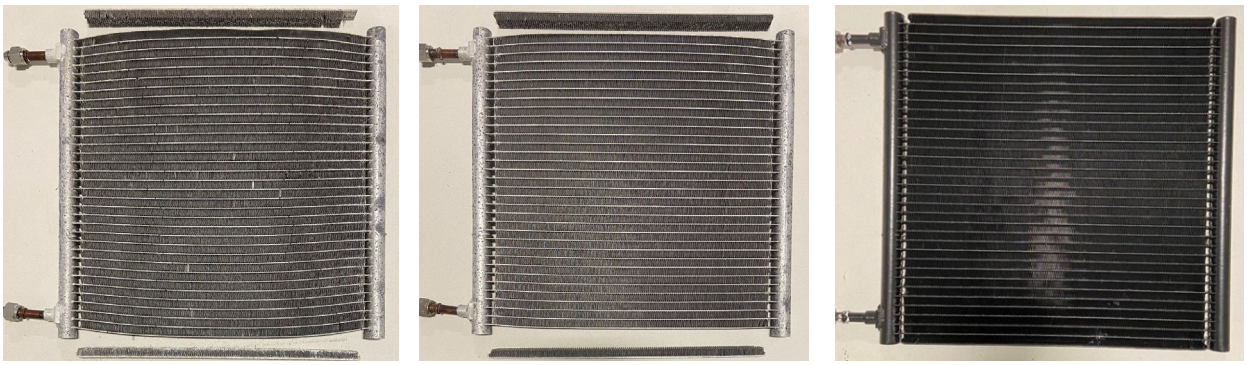

(a) Bare HX (b) TCP-coated HX (c) E-coated HX

Figure 4: Three MCHEs after ten days of exposure to SWAAT: (a) bare HX; (b) TCP-coated HX; (c) e-coated HX

Figure 6 shows the representative pictures of fins of three MCHEs at different stages of the experiments: (1) before the corrosion test, (2) after the corrosion test and before cleaning, and (3) after cleaning. It can be seen that after the corrosion test (before cleaning), a large amount of deposit (salt and/or corrosion products) is observed on both the bare and TCP-coated HXs. Only a very small amount of deposit can be found on the E-coated HX. After the cleaning procedure, the surface deposit is removed. Damage to fins, tubes, and brazed joints due to corrosion, if any, can be revealed. Exfoliation and loss of aluminum material are visually observed on the edge of fins on bare HX. No apparent surface damage can be visually observed on the fins of TCP-coated and e-coated HX. The fins of bare HX deform during the SWAAT test. It is speculated that the accumulation of salt and corrosion products between the deboned fins and tubes is related to both the overall HX deformation and fin deformation.

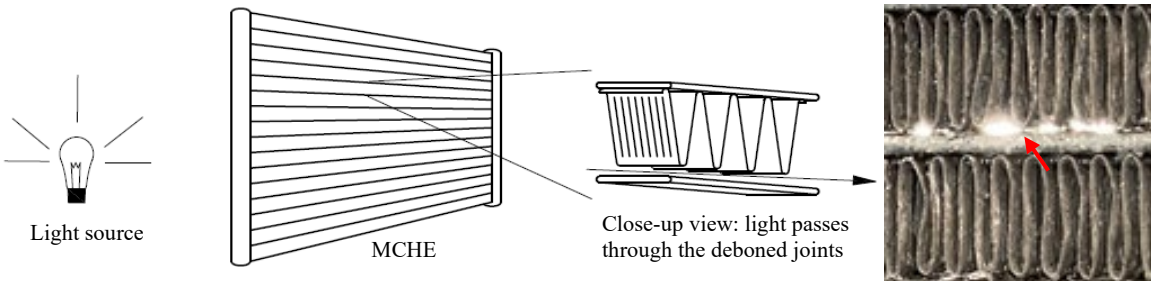

Figure 5: Observation of complete deboned fins and tubes with the assistance of a light source

Time of inspection	Bare MCHE	TCP-coated MCHE	E-coated MCHE
Before SWAAT	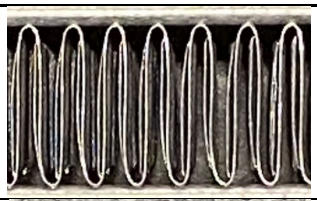	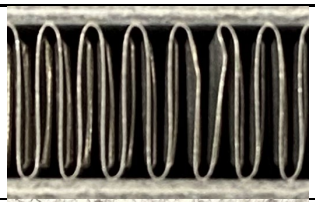	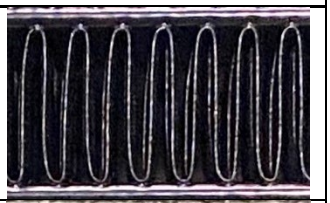
After SWAAT (uncleaned)		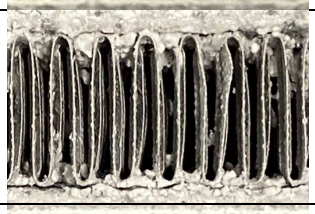	
After SWAAT (cleaned)	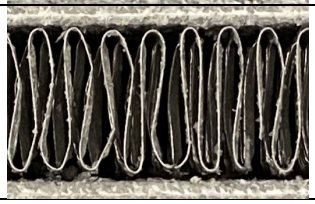	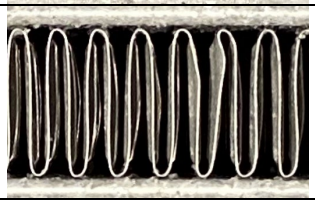	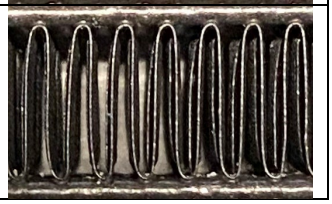

Figure 6: Fins of three MCHEs before and after the SWAAT (before and after the cleaning)

3.2 Thermal-hydraulic performance of the MCHEs before and after corrosion tests

The results of the thermal-hydraulic performance evaluation before the corrosion tests are shown in Figure 7. At the same air flow rate, no distinct difference in the *UA* of three MCHEs is observed (Figure 7(a)). The airside pressure drop of bare and TCP-coated HXs are very close to each other. The airside pressure drop of the e-coated HX is up to 19% higher than the other two HXs (Figure 7(b)). The measurement results indicate that the thin chromium conversion coating does not impact the thermal-hydraulic performance of the HX significantly. For the e-coated HX, The relatively thicker coating leads to a decrease in the free flow area. Therefore, a higher free flow air velocity and the airside pressure drop are expected and confirmed by the experimental results. Although the increase in the free flow air velocity will lead to an increase in the heat transfer coefficient, the non-metal e-coating layer also led to an increase in the thermal resistance of the fins. The opposite effects on heat transfer result in little difference in *UA* of the e-coated HX vs. the other evaluated HXs. To estimate the penalty on system efficiency due to the higher pressure drop when using the e-coated heat exchanger, the UA values are compared at the same theoretical fan power (Eq.8), as illustrated in Figure 8. It is found that the *UA* of the e-coated HX is slightly lower than the bare HX by 2%.

$$\dot{W}_{fan} = \Delta P_a \cdot \dot{V} \tag{8}$$

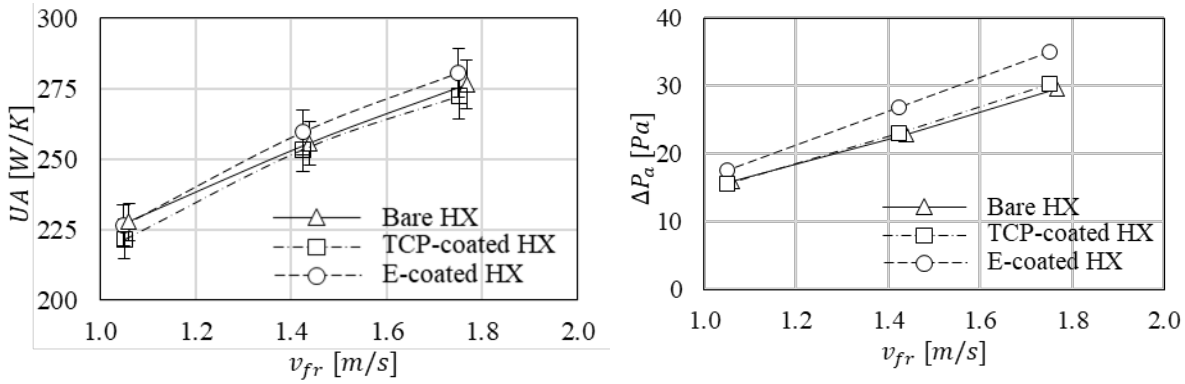

(a) (b)

Figure 7: Thermal-hydraulic performance of three MCHEs before the SWAAT: (a) similar *UA* of all examined MCHEs; (b) the airside pressure drop of E-coated HX is higher than the bare and TCP HXs

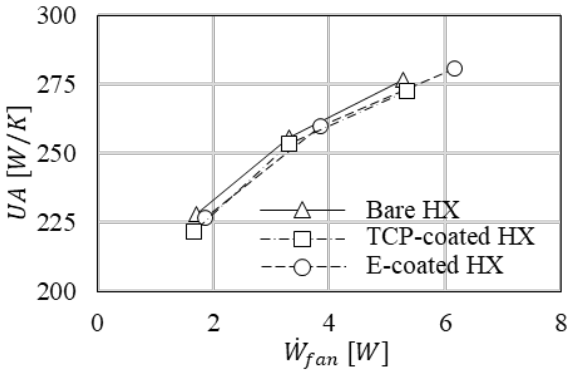

Figure 8: *UA* of three MCHEs vs. theoretical fan power before the SWAAT

After the ten-day corrosion tests and the cleaning processes, the thermal-hydraulic performance of all three MCHEs is evaluated again. Due to the deformation of bare and TCP-coated HX, and the loss of top/bottom fin rows as illustrated in Figures 4(a)&(b), the front areas of these two HXs have changed, therefore, the airflow rate of these HXs is adjusted accordingly to maintain the same frontal face velocity. Figure 9 shows the airside pressure drop of three MCHEs before and after the corrosion tests. It is found that the airside pressure drop of bare HX increases by up to 13% after the corrosion test, at around 1.8m/s frontal air velocity (Figure 9(a)). The increase of the pressure drop may be contributed by a few factors: (1) The deformation of fins; (2) The change in the surface condition of the HX due to corrosion. The airside pressure drop of the TCP-coated HX decreases by up to 3% after the corrosion test (Figure 9(b)). The airside pressure drop of e-coated HX decreases by up to 5.6% after the corrosion test (Figure 9(c)). The

changes in pressure drop of the TCP-coated and e-coated heat exchangers are relatively small compared to the bare heat exchanger. This may be related to the fact that there is less or no deformation of the fins on TCP-coated and e-coated HXs..

The *UA* of three evaluated MCHEs before and after the corrosion tests is shown in Figure 10. As shown in Figure 10(a), the *UA* of the bare HX decreases by around 73% after the corrosion test. One major cause of such a significant decrease in thermal performance is the fin/tube debonding due to the corrosion of the brazed fin/tube joints. Basically, the detached fins cannot serve as an efficient heat transfer surface. At the locations where fins are still bonded to the tube, the change of surface feature due to corrosion may also contribute to the loss of heat transfer performance of HXs (Wang *et al*., 2021). The *UA* of the TCP-coated HX also shows a large decrease of around 60% after the corrosion test, see Figure 10(b)). Similar to the bare HX, the thermal performance degradation is closely related to the fin/tube debonding in this HX. Based on the visual examination (Figure 5), the percentage of the completely lost braze joints in the TCP HX (21%) is smaller than the bare HX (33%), which may have contributed to the slightly better thermal performance of the TCP HX than the bare HX after corrosion tests. The results indicate that protection of the braze joints is critical for preserving the thermal performance of MCHEs in long term. Another factor that may have contributed to the more severe decrease in *UA* of bare HX is the corrosion of fins. Based on the visual observation of the fins at the frontal face of bare and TCP-coated HXs, the fins of bare HX seem to be affected more than the fins of TCP-coated HX, as shown in Figure 6. A more detailed examination of the fins of these two HXs will be conducted in future work to confirm this speculation. The change of *UA* of e-coated HX is insignificant (up to 3% at a frontal velocity of 1.05 m/s) after the corrosion test and within the range of experimental uncertainty (Figure 10(c)). The e-coating shows a good corrosion resistance to the SWAAT environment. However, the results of the relatively unchanged thermal-hydraulic performance of e-coated HX may not be directly used to predict the HX performance in real-life service since other aspects of the coating degradation have not been considered in the current testing procedure. In the future study, real-life factors such as HX fatigue during operation, and the other environmental conditions may be considered.

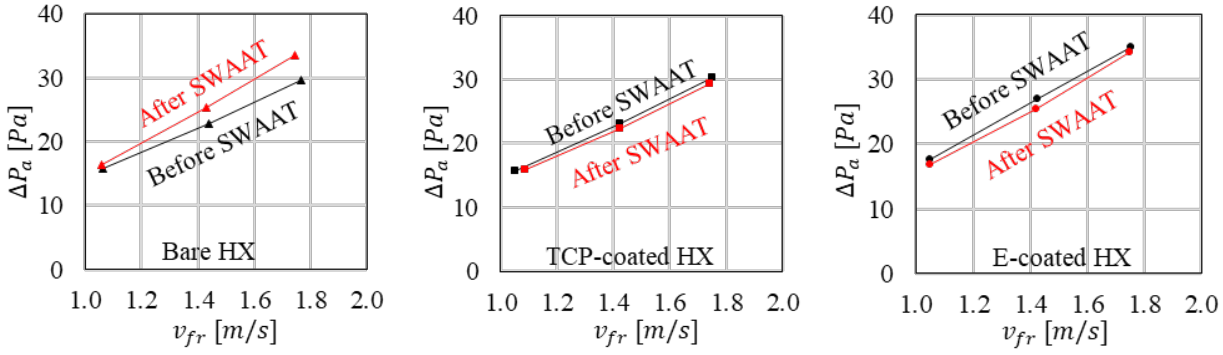

Figure 9: Airside pressure drop of three MCHEs before and after the SWAAT (cleaned): (a) increased airside pressure drop of bare HX; (b)(c) slightly reduced airside pressure drop of TCP-coated and E-coated HXs

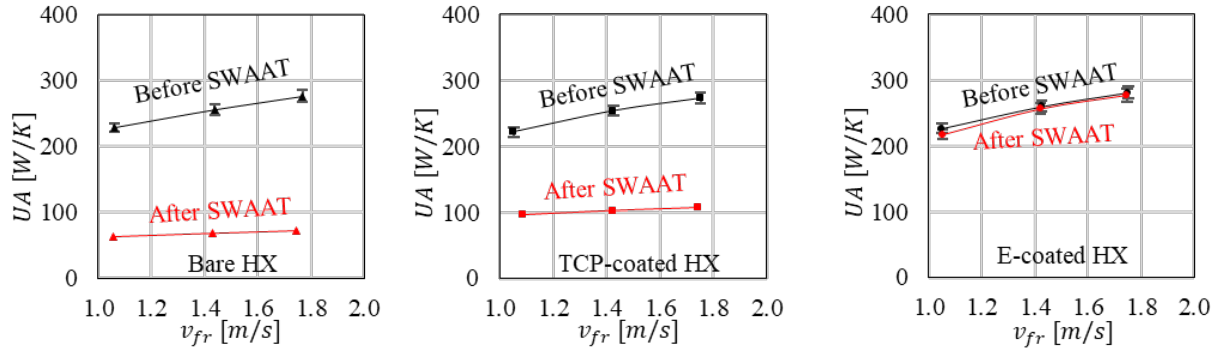

Figure 10: *UA* of three MCHEs before and after the SWAAT (cleaned): (a) significantly reduced *UA* of the bare HX; (b) significantly reduced UA of the TCP-coated HXs; (c) slightly reduced *UA* of the E-coated HX

4. CONCLUSIONS

In this study, the corrosion behavior of three otherwise identical MCHEs with different surface treatments, i.e. no coating, TCP coating, and e-coating, is evaluated under the effects of a ten-day SWAAT corrosion test. The thermal-hydraulic performance of all three MCHEs is evaluated before and after the corrosion tests.

Before the corrosion tests, the e-coating shows a bigger impact on the thermal-hydraulic performance of the MCHE than the TCP coating. The e-coated HX has an up to 19% higher airside pressure drop than the uncoated bare HX at the same frontal velocity (Figure 7(b)). At the same fan power, the e-coated HX shows a 2% lower *UA* than the bare HX (Figure 8). The TCP-coated HX does not show a significant difference in the airside pressure drop or *UA* from the bare HX (Figure 7(a)&(b)).

After the ten-day SWAAT corrosion test, the bare HX shows severe deformation and loss of brazed joints. The TCP heat exchanger also shows some deformation and loss of brazed joints. The e-coated HX shows overall good corrosion resistance under the current laboratory corrosion test.

The airside pressure drop of the bare HX increases by up to 13% (Figure 9(a)) and the *UA* decreases by around 73% (Figure 10(a)) after the corrosion test, as a result of corrosion. the TCP coating shows limited ability to preserve the mechanical integrity and thermal-hydraulic performance of the MCHEs after the accelerated corrosion tests. The airside pressure drop of the TCP-coated HX does not change significantly after the corrosion test (Figure 9(b)). However, a 60% decrease in *UA* of the TCP-coated HX is measured after the corrosion test. For both the bare HX and TCP HXs, the large decrease of UA is related to the significant loss of brazed joints due to corrosion.

The e-coating HX shows insignificant changes in thermal-hydraulic performance after the current ten-day laboratory corrosion test. However, the impact of many real-life conditions remains to be studied.

NOMENCLATURE

A	Heat transfer area	[m^2]	**Subscript**	
c_p	Specific heat at constant pressure	[$J \cdot kg \cdot K^{-1}$]	*a*	Air side
C	Flow-stream capacity rate	[$J \cdot K^{-1} \cdot kg^{-1}$]	*w*	Water side
h	Enthalpy	[$J \cdot kg^{-1} \cdot K^{-1}$]	*n*	Nozzle
$\dot{M}$	Mass flow rate	[$kg \cdot s^{-1}$]	*i*	Inlet
NTU	Number of transfer unit	[-]	*o*	Outlet
P	Pressure	[Pa]	*fr*	Frontal face of heat exchanger
$\dot{Q}$	Rate of Heat transfer	[W]	*fan*	Air blower fan
T	Temperature	[°C]	*max*	Maximum
U	Overall heat transfer coefficient	[$W \cdot m^{-2} \cdot K^{-1}$]	*min*	minimum
v	Velocity	[$m \cdot s^{-1}$]		
$\dot{V}$	Volumetric velocity	[$m^3 \cdot s^{-1}$]		
$\dot{W}$	Rate of work	[W]		
ε	Heat exchanger effectiveness	[-]		

ACKNOWLEDGMENT

The authors would like to thank the member companies of the Air Conditioning & Refrigeration Center at the University of Illinois at Urbana-Champaign for their financial support, as well as Creative Thermal Solutions, Inc. (CTS) for providing testing facilities, and CTS employees for their technical support.

REFERENCES

Ainali, M., Sundberg, R., & Miner, D.K. (1993). Electrocoating of Car Radiators – A way to Improve Corrosion Resistance. *SAE Technical Papers*. DOI: 10.4271/931108

American Society for Testing and Materials. (2011). *Standard Practice for Modified Salt Spray (Fog) Testing*. https://doi.org/10.1520/G0085-11

American Society of Heating, Refrigerating and Air-Conditioning Engineers. (2018). *Standard Methods for Air Velocity and Airflow Measurement*.

Fedrizzi, L., Andreatta, F., Paussa, L., Deflorian, F., & Maschio, S. (2008). Heat exchangers corrosion protection by using organic coatings. *Progress in Organic Coatings, 63(3)*, 299–306. https://doi-org.proxy2.library.illinois.edu/10.1016/j.porgcoat.2008.01.009

Qi, J.-T., Hashimoto, T., Walton, J. R., Zhou, X., Skeldon, P., & Thompson, G. E. (2015). Trivalent chromium conversion coating formation on aluminium. *Surface and Coatings Technology*, 280, 317–329. DOI: 10.1016/j.surfcoat.2015.09.024

Scott, A., Woods, R., & Harris, J. (1991). Accelerated corrosion test methods for evaluating external corrosion resistance of vacuum brazed aluminum heat exchangers. *SAE Transactions, 100*, 578–586.

Walton, J., Shruthi, T. K., Swain, G. M., Yancey, D., Vlasak, P., & Westre, S. (2019). Evaluation of a trivalent chromium process (TCP) conversion coating on AA2024-T3 that requires no surface pretreatment. *Journal of the Electrochemical Society*, 166(15), C589–C599. DOI: 10.1149/2.0881915jes

Wang, Y.P., Zhao, H., Hrnjak, P. (2021, May) An Evaluation of the Effect of Corrosion Tests on Thermal Performance of Aluminum Heat Exchangers. *18th International Air Conditioning and Refrigeration Conference at Purdue*, West Lafayette, IN

Melander, M., & Woods, R. (2010). Corrosion Study of Brazed Aluminum Radiators Retrieved from Cars After Field Service. Corrosion, 66(1), 0150051-01500514. DOI: 10.5006/1.3318283

Mills, A. F. (1999). *Heat transfer* (2nd ed.). Prentice-Hall.

Munson, C. A., & Swain, G. M. (2017). Structure and chemical composition of different variants of a commercial trivalent chromium process (TCP) coating on aluminum alloy 7075-T6. *Surface and Coatings Technology*, 315, 150–162. DOI: 10.1016/j.surfcoat.2017.02.018

Munson, C. A., McFall-Boegeman, S. A., & Swain, G. M. (2018). Cross comparison of TCP conversion coating performance on aluminum alloys during neutral salt-spray and thin-layer mist accelerated degradation testing. *Electrochimica Acta*, 282, 171–184. DOI: 10.1016/j.electacta.2018.04.115